Theoretical Study of the Influence of Monomer Excess on the Structure and Properties of Polyaniline Oligomers

Anela N. Ivanova,[†,‡] Alia V. Tadjer,[*,†] and Natalia P. Gospodinova[‡]

Faculty of Chemistry, University of Sofia, 1 J. Bourchier Avenue, 1126 Sofia, Bulgaria, and Laboratoire de Chimie Macromoléculaire, Ecole Nationale Supérieur de Chimie de Mulhouse, 3, rue Alfred Werner, 68093 Mulhouse Cedex, France, Institut de Chimie des Surfaces et Interfaces, 15, rue Jean Starcky, BP 2488, 68057 Mulhouse Cedex, France

Received: October 28, 2005; In Final Form: December 6, 2005

Polyaniline is among the most intensely investigated polymers because of its exceptional properties affording its current and potential applications. The structure and energy spectra of isolated oligomers and infinite chains in different oxidation states and degrees of protonation have been discussed at length from experimental and theoretical perspectives. The reaction environment effect, however, has received less attention and, particularly, the influence of monomer excess has been completely neglected in theoretical studies. Experimental measurements show that residual aniline is always detected in emeraldine samples obtained at low pH. Upon addition of oxidant to emeraldine PANI samples, post-polymerization due to the presence of excess monomers occurs. This is an indication of the formation of aniline−PANI complexes in the reaction medium. The presence of aniline monomers should affect the PANI chain arrangement and optical/conducting characteristics. Therefore, model clusters of aniline with neutral or singly protonated emeraldine tetramers in explicit water medium and periodic boundary conditions are addressed in this paper using a Monte Carlo/AMBER96/AM1 computational protocol to simulate the absorption spectra. The monomer impact on the structure, energy characteristics, and UV/vis spectra of the polymer are discussed.

Introduction

Among all π-conjugated organic polymers, polyaniline (PANI) is the one possessing the widest diversity of properties ranging from dc conductivity ($\sim 10^2$ S/cm at ambient conditions),[1−3] through a variety of colors depending on the oxidation state of the nitrogen atoms,[4−7] to magnetic activity[1,2,8−10] and ability to form various supramolecular assemblies with high potential for applications.[11−14] Nonetheless, PANI is obtained easily in aqueous medium, which opens new routes for biologically oriented implementations.[15−17] The most substantial amount of research devoted to polyaniline is focused on understanding the mechanism of electron transport and conductivity[1−3,18−21] and the optical properties[4] of its various forms. A number of theories are proposed for explanation of the accumulated experimental data.[1,9] The most intriguing PANI form is the doped emeraldine salt (ES), which is the conducting state of PANI, and its deprotonated analogue, the emeraldine base (EB). Polymerization of aniline is usually performed at very low pH values (<2.0) provided by the presence of a strong (doping) acid. The reaction proceeds quickly to give a green product ($\lambda_{max} \approx 800$ nm), considered to be the ES. Upon increase of pH (>5.0) the reaction mixture turns blue ($\lambda_{max} \approx 650$ nm, presumed to be EB).

However, the exact structure−property correlation at the molecular level is still missing. Although various microscopic and spectroscopic techniques[20,22−24] are applied for studying PANI's structure and organization, the acquired knowledge remains at the mesoscopic level because of technical limitations or the inability of PANI to form long-range crystalline domains.[18,22,25]

Therefore, information from molecular modeling is essential for elucidating the microscopic structure of polyaniline chains and its reflection in different PANI characteristics.

A number of communications tackle quantum chemical models of isolated PANI oligomers of different lengths and oxidation states.[26−30] They discuss geometry, electronic structure, conductivity, and optical absorption of various oligomers ranging from dimers to dodecamers. However, all models suffer from a common deficiency: the studied oligomers are either phenyl- or amino-capped in order to ensure higher symmetry and thus reduce computational time. There are few studies[26,31] reporting quantum chemical modeling of the intermolecular interaction of PANI oligomers, but the simulations are performed in vacuum and with end-capped models. As far as solvent effect is concerned, the only models reported treat interaction of PANI oligomers with a limited number (up to five) of solvent molecules.[26,27,29]

In a previous study,[32] we have attempted to improve the models of single PANI oligomer chains by investigating oligomers with the proper translational symmetry; the environment and the intermolecular interactions are accounted for by studying clusters of oligomers dissolved in water and/or stacked on top of each other. The results of the simulated optical spectra can be summarized as follows. Water always has a weak hypsochromic effect on the longest wavelength transition (LWT) in the optical spectra. On the contrary, the presence of a second oligomer results in two special features: the absorption maximum of the single hydrated oligomer does not change its position but the intensity of the transition increases appreciably.

* Corresponding author. E-mail: tadjer@chem.uni-sofia.bg. Tel: ++359-2-8161374. Fax: ++359-2-9625438.
† University of Sofia.
‡ Ecole Nationale Supérieur de Chimie de Mulhouse.

10.1021/jp056206+ CCC: $33.50
Published on Web 01/21/2006

However, a less intensive, markedly bathochromic peak (shifted by 50−100 nm relative to the single tetramer) appears in all cases. Protonation leads to a new visible transition, corresponding to intramolecular charge transfer for pernigraniline (PNB) and to intermolecular CT for singly protonated emeraldine. Hence, the redshift is more pronounced in PNB than in singly protonated emeraldine (SPE) clusters.

The latter trend, however, contradicts the experimental spectra in which protonated emeraldine absorbs at ∼800 nm, while the LWT of both protonated and neutral PNB is ∼540 nm. Possible reasons may be the insufficient degree of protonation in emeraldine or the presence of other molecules in the reaction medium, for example, aniline monomers, which affect the optical properties of PANI. Moreover, knowledge about the effect of the stacking interaction between aniline and emeraldine will provide more insight into the optical spectra recorded during polymerization because the excess of monomer in the reaction mixture is inevitable. As the oxidant/aniline ratio seems to be a crucial condition for complete aniline exhaustion, earlier we have performed measurements of electrochemical potential, E, with absorption spectra recording during stepwise addition of oxidant to PANI suspension characterized by $\lambda_{max} \approx 800$ nm and $E \approx 0.25$ V (vs SCE), respectively.[33] Upon adding of oxidant, both E and λ_{max} are changed instantly ($E \approx 0.75$ V and $\lambda_{max} \approx 540$ nm), followed by "relaxation" to $E \approx 0.25$ V and $\lambda_{max} \approx 800$ nm. These changes do not occur only upon addition of a very high excess of oxidant (molar ratio of oxidant to initial aniline concentration of about 2.4). The same post-polymerization is observed upon adding of oxidant to the PANI suspension obtained at initial oxidant/monomer molar ratio of 1.5 and dialyzed for 1 week.

The very presence of residual monomer as a prerequisite for post-polymerization is the most likely explanation for the well-known stability of the PANI emeraldine form (absorbing at 800 nm) in a wide potential range (0.2−0.5 V vs SCE).[34] The absence of residual monomer in PANI films prepared using the Langmuir−Blodgett technique results in production of PANI characterized by $\lambda_{max} \approx 540$ nm.[35,36]

The presence of aniline monomers should affect the PANI chain arrangement and optical/conducting characteristics. The occurrence of PANI−aniline clusters in the reaction solution is even more likely at the early stages of polymerization when the aniline/oligomer ratio is still very high.

To study this effect, we construct a number of models consisting of one PANI tetramer in the emeraldine oxidation state interacting with one aniline molecule. The impact of aniline on the arrangement and properties of hydrated emeraldine oligomers upon protonation is monitored as well. Analysis of the results in terms of structure, energy, and electronic absorption spectra is provided.

Molecular Models and Computational Scheme

We limit our research to neutral and singly protonated emeraldine oligomers (Figure 1). The models we build comprise one PANI tetramer (EB or SPE), one monomer molecule (ANI), and a counterion where necessary to keep the system neutral. Figure S1 represents the different types of clusters considered.

All of the clusters studied are dissolved in water (not shown in the Figures). The aqueous environment is built of water molecules (140 and 170 water molecules in the EB and SPE clusters, respectively) and is created by the periodic box tool[37] implemented in the Hyperchem 7 package.[38] The size of the periodic box is $18 \times 18 \times 30$ Å^3. The chosen number of water molecules is in the range of concentrations used in the experiments and allows the formation of at least two solvent "shells" around the PANI tetramers and even more around the counterions where present. This is a prerequisite for reliability of the calculations. All of the systems are treated in periodic boundary conditions to simulate continuous solution.

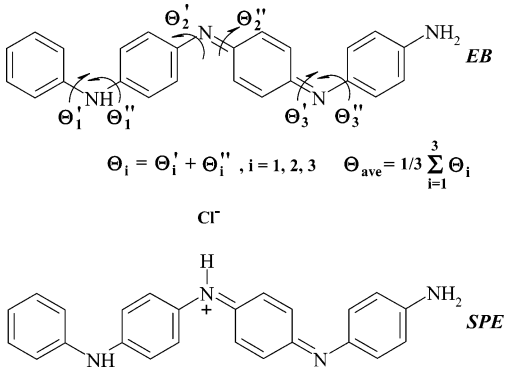

Figure 1. Chemical formulas of the modeled emeraldine oligomers with notation of the torsion angles.

A combined Monte Carlo/molecular mechanics technique is employed for low-energy structures sampling. The hydrated PANI tetramers are subjected to Monte Carlo simulation based on the Metropolis scheme[39] for acceptance of low-energy configurations. The energy of the structures is calculated with the AMBER96 force field.[40] All water molecules are explicitly included in the calculation and are described with the TIP3P model.[41] The AMBER96 force field is chosen as being the most appropriate (from the available set) for calculations of conjugated aromatic systems such as PANI. Further computational details are provided in the Supporting Information.

After equilibration of the Monte Carlo simulations (25 000 to 30 000 steps depending on the system, cf. Supporting Information), a series of 15 lowest-energy configurations are selected from the relaxed part of each Monte Carlo trajectory for further optimization and characterization.

The geometry of each series of lowest-energy clusters for every topology is fully optimized (PANI and water) with AMBER 96. The optimized structure (see the Supporting Information for optimized bond lengths, dihedral angles, and comparison to structures reported by other authors) is used for structural analysis and optical spectra simulation. All of the values shown below are averaged over the entire series. The absorption spectra are calculated for the set of PANI tetramer (with counterions where present) and aniline molecules only. The aqueous environment is treated as a fixed point-charge enveloping field in spectra computation. This is reasonable because the interest is focused mainly on the visible absorption of PANI. The UV/vis spectra are obtained with AM1/CIS (24,23) (the active space comprises 24 electrons in 23 orbitals) for EB−ANI and AM1/CIS(26,26) for SPE−ANI. The size of the active space is selected on the basis of two criteria: lack of MO degeneracy at the terminal orbitals and inclusion of the same number of π orbitals in the simulations. The above active spaces satisfy the nondegeneracy requirement and involve 20 π-MOs in the spectra simulations.

Results and Discussion

1. Emeraldine Base/Aniline Clusters. The interaction of the aniline monomer with the PANI tetramers will depend on their mutual orientation. Therefore, several clusters with differing alignment of the aniline molecule on top of an EB tetramer are calculated. A schematic representation of all structures is shown in Figure 2.

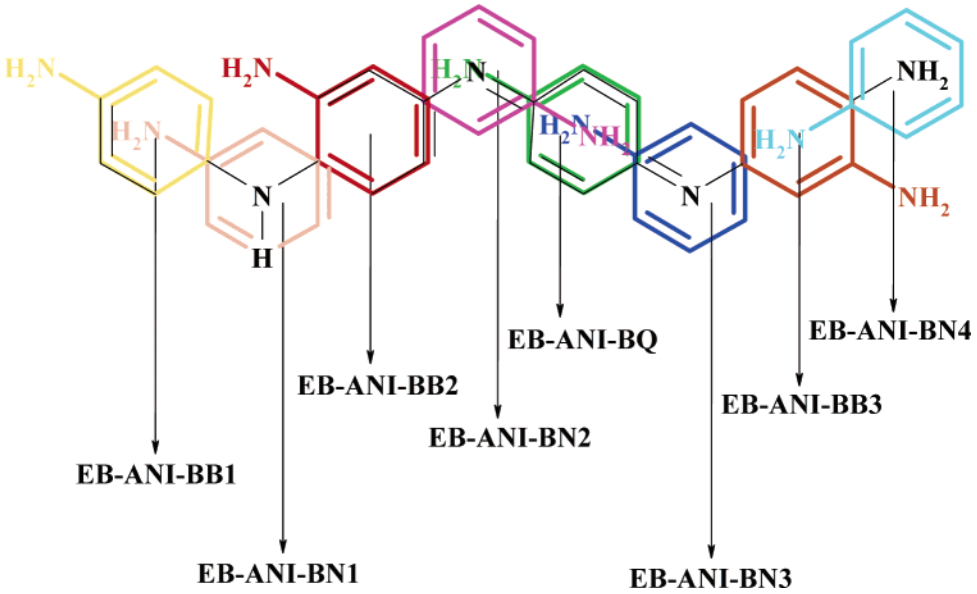

Figure 2. Scheme of the studied EB−ANI clusters. Different colors of the aniline molecule correspond to different alignments with respect to the tetramer.

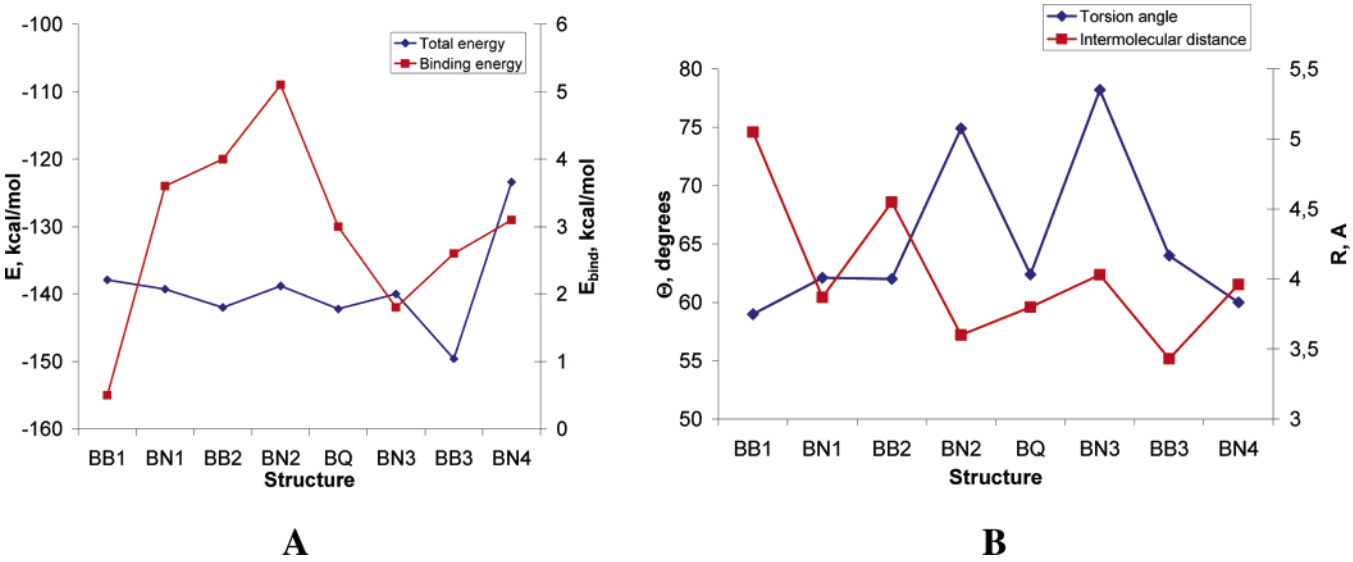

Figure 3. Plots of total and binding energy (A) and torsion angle and intermolecular distance (B) as a function of aniline position in EB−aniline stacks.

The position of aniline with respect to the tetramer is chosen to correspond to minimum electrostatic repulsion (based on AM1 charge estimates), that is, the largest negative atomic charges in aniline are directly on top of the largest positive atomic charges in the tetramer and vice versa.

The eight structures shown in Figure 2 are subjected to the Monte Carlo/molecular mechanics computational procedure described in the previous section. The obtained structural parameters, averaged over the AMBER96 optimized geometries, are summarized in Table 1 and Figures 3 and 4.

The total energy of the stack (E) is the energy of the EB (SPE) tetramer−aniline stack (and counterion where present) in water calculated for the AMBER96 optimized geometries and averaged over the series of 15 optimized structures.

The binding energy (E_{bind}) between EB (SPE, see Table 3) and aniline is estimated as follows

$$E_{bind} = E - (E_{EB(SPE)} + E_{ANI})$$

where E is the total energy of the hydrated stack, $E_{EB\ (SPE)}$ is the energy of the EB (SPE) tetramer, and E_{ANI} is the energy of aniline from the same stack. We believe that this way for evaluation of the binding energy reflects more correctly the specific interaction in the given stack than the energy difference

TABLE 1: Average AMBER96 Total Energy of the Stack (E), Binding Energy (E_{bind}), Torsion Angle (Θ_{ave}) and Intermolecular Distance (R) for Clusters of Emeraldine Base Tetramers with Aniline in Water[a]

structure	E, kcal/mol	E_{bind}, kcal/mol	Θ_{ave}, deg	R, Å
EB−ANI−BB1	−137.9 (4.2)	0.5 (0.4)	59.0 (4.0)	5.05 (0.09)
EB−ANI−BN1	−139.3 (3.5)	3.6 (0.3)	62.1 (2.0)	3.87 (0.03)
EB−ANI−BB2	−142.0 (2.5)	4.0 (0.5)	62.0 (3.2)	4.55 (0.11)
EB−ANI−BN2	−138.8 (2.3)	5.1 (0.2)	74.9 (3.2)	3.60 (0.06)
EB−ANI−BQ	−142.2 (4.1)	3.0 (0.3)	62.4 (2.2)	3.80 (0.11)
EB−ANI−BN3	−140.0 (2.9)	1.8 (0.3)	78.2 (2.3)	4.03 (0.06)
EB−ANI−BB3	−149.6 (3.2)	2.6 (0.2)	64.0 (2.4)	3.43 (0.02)
EB−ANI−BN4	−123.4 (6.1)	3.1 (0.2)	60.0 (2.9)	3.96 (0.17)

[a] The values are averaged over a series of 15 optimized hydrated clusters for each structure. The standard deviations are given in brackets.

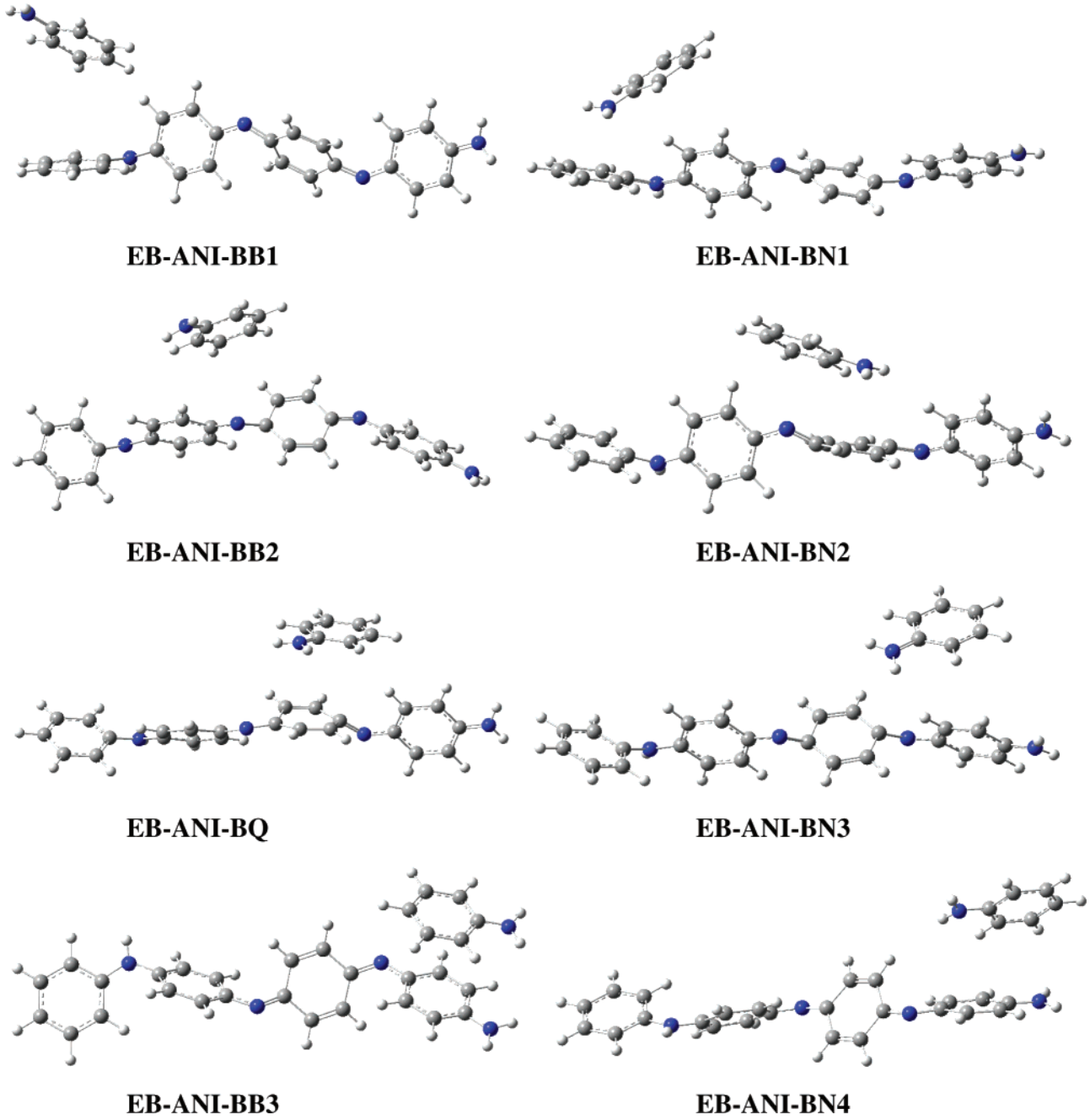

Figure 4. Examples of AMBER96 optimized structures of EB−aniline stacks with different alignment of the aniline molecule with respect to the EB tetramer. The water molecules are not shown.

obtained by separate simulations of the respective counterparts of the stack. The scheme used in our study can be regarded as analogous to the counterpoise correction of the BSSE in ab initio quantification of binding energies. It is known that this correction yields much more accurate binding energies because it ensures an identical "environment" of the two subparts upon calculation of their energies by keeping the conditions of the entire cluster constant.

The angle Θ is an average value of the torsion angle between each pair of adjacent benzene rings (Figure 1) in the optimized tetramers in the clusters and R is the average distance between the molecules of aniline and EB. It is estimated by averaging over a number of close-contact atomic pairs from the two molecules.

The optimized structures show that there is a pronounced tendency for displacement of the aniline cycle from facing directly any tetramer cycle. The aniline molecule is coplanar with the quinoid ring only in the EB−ANI−BQ cluster. In the other structures, there is a substantial tilt of aniline with respect to the plane of the nearest ring. All of the optimized geometries except EB−ANI−BB3 correspond to positioning of the benzene ring of aniline on top of one of the tetramer nitrogen atoms. In EB−ANI−BB3, the benzene ring of aniline is substantially displaced from its counterpart in the tetramer and the aniline nitrogen is pointing out to the water.

The structures considered are not equivalent in energy, but the differences in total energy of the stacks are not very broad; the energy variation between the most and the least stable alignments is 26.2 kcal/mol. This means that there will be nonzero probability for the existence of all structures in the reaction environment. In terms of total energy, the most stable is EB−ANI−BB3, which also features the smallest intermo-

TABLE 2: AM1/CIS Calculated UV/Vis Spectra of EB−Aniline Stacks in Water[a]

structure	λ, nm	f	MOs	E_{HOMO}, eV	Θ_{QA}, deg
EB−ANI−BB1	545 (12) 441 (8)	1.272 (0.080) 0.035 (0.035)	HOMO → LUMO HOMO−2 → LUMO HOMO−3 → LUMO	−7.418	46.34
EB−ANI−BN1	687 (40) 527 (26)	0.961 (0.188) 0.057 (0.045)	HOMO → LUMO HOMO−2 → LUMO	−7.126	71.05
EB−ANI−BB2	607 (42) 441 (11)	0.902 (0.148) 0.248 (0.060)	HOMO → LUMO HOMO−2 → LUMO	−7.228	67.86
EB−ANI−BN2	621 (38) 493 (26)	0.806 (0.151) 0.129 (0.057)	HOMO → LUMO HOMO−1 → LUMO HOMO−3→ LUMO	−7.645	60.99
EB−ANI−BQ	775 (107) 474 (14)	0.573 (0.139) 0.589 (0.165)	HOMO → LUMO HOMO−1 → LUMO	−7.086	82.39
EB−ANI−BN3	750 (39) 547 (24)	0.615 (0.084) 0.213 (0.078)	HOMO → LUMO HOMO−1 → LUMO	−7.081	85.87
EB−ANI−BB3	596 (20) 478 (16)	1.037 (0.077) 0.025 (0.029)	HOMO → LUMO HOMO−2 → LUMO	−7.240	63.19

[a] Only the wavelengths (λ) of the transitions in the visible region are presented. f is the oscillator strength. The values are averaged over series of 15 optimized hydrated clusters for each structure. The standard deviations are given in brackets. The fourth column contains the configurations with the largest coefficients involved in the corresponding transition. The last two columns comprise the energy of the HOMO orbital and the values of the torsion angle between the quinoid and the relevant (A2 or A3) adjacent aromatic ring (Θ_{QA}) (see the text).

TABLE 3: Average AMBER96 Total Energy of the Stack (E), Binding Energy (E_{bind}), Torsion Angle (Θ), Intermolecular Distance (R), and Chloride−Proton Distance ($r_{H...Cl}$) for Clusters of Singly Protonated Emeraldine Tetramers with Aniline in Water[a]

structure	E, kcal/mol	E_{bind}, kcal/mol	Θ, deg	R, Å	$r_{H...Cl}$, Å
SPE−ANI−BB2	−363.6 (4.7)	3.9 (1.4)	65.4 (2.6)	5.97 (0.16)	3.25 (0.13)
SPE−ANI−BN2	−389.3 (5.5)	−0.6 (0.3)	63.6 (3.3)	3.31 (0.03)	3.90 (0.10)
SPE−ANI−BQ	−355.1 (4.0)	6.6 (0.8)	47.0 (2.3)	3.46 (0.13)	3.02 (0.13)

[a] The values are averaged over a series of 15 optimized hydrated clusters for each structure. The standard deviations are given in brackets.

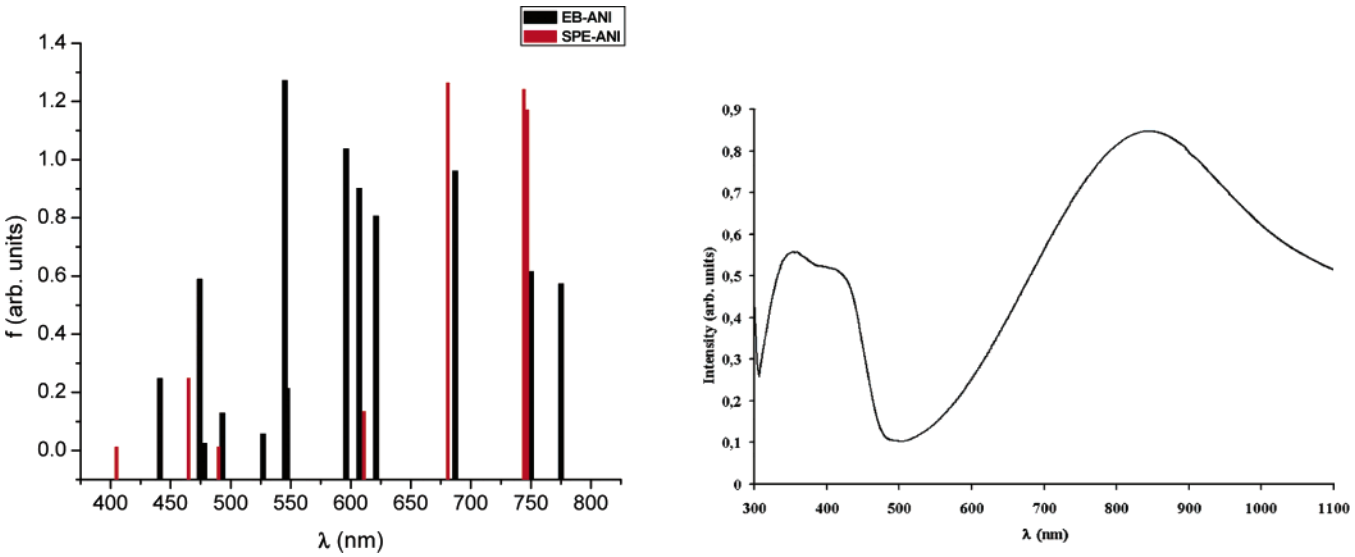

Figure 5. AM1/CIS calculated absorption spectra of EB−ANI (black bars) and SPE−ANI (red bars) hydrated clusters (left). λ is the absorption wavelength in nm, and f is the oscillator strength of the transition. Experimental UV/vis/NIR absorption spectrum of polyaniline adsorbed on a mica sheet (right).

lecular distance. The stabilization may be due to two factors: (i) no direct overlap of carbon atoms from the aromatic cycles and (ii) enhanced hydration of the aniline nitrogen, which is not screened directly by any of the tetramer atoms (rings).

All of the calculated values of the binding energy, however, are positive, which means that the packing forces between aniline and the EB tetramer are repulsive. This is an indication that the overall stabilization of the clusters is due to effective hydration. The least repulsive values of the binding energy, that is, in EB−ANI−BB1 and EB−ANI−BN3, correspond to minimized screening of the two molecules, which is an implication that tightly packed stacks of EB and aniline will not form spontaneously.

The presence of aniline in the vicinity of the EB tetramer perturbs the structure of the latter in various ways as well. The calculated intermolecular distances vary between 3.4 and 5.0 Å, which is typical for aromatic stacks.[42] As should be expected, the intermolecular separation is largest in terminal structure EB−ANI−BB1 because of the reduced overlap and decreases when aniline is moved to the core of the tetramer. The obtained R

value is similar to those calculated for stacks consisting of two EB tetramers.[32]

The variation of the average torsion angle as a function of the aniline position shows somewhat opposite trends. The least twisted structures correspond to positions of aniline at the two ends of the tetramers. However, the values are still larger than the average value for a single hydrated EB tetramer (50.0°[32]). The most discernible twist is observed when aniline interacts with the two imine nitrogen atoms, where the angles are >70°. In all other structures, the calculated twisting is ~60°, which is similar to the one obtained for stacks of two EB tetramers.[32]

The perturbation in the tetramer structure is reflected in the calculated UV/vis absorption spectra, which are summarized in Table 2 and Figure 5. In all cases, there is a pronounced bathochromic shift of the LWT with respect to a single hydrated EB tetramer (λ_{max} = 521 nm[32]). The redshift is even stronger than that observed in the stacks of two tetramers (λ_{max} = 598 nm and λ_{max} = 657 nm[32]). Only λ_{max} of EB−ANI−BB1 is close to the latter values, which is due to the negligible EB−aniline interaction.

Unlike the stacks of two EB tetramers, in the EB−ANI systems the longest-wavelength transition remains the most intensive one, except in EB−ANI−BQ, where the two visible transitions have almost equal oscillator strengths. The values obtained for the EB−aniline clusters are much closer to the experimental spectra as well. The LWT is a HOMO → LUMO transition, which corresponds to transfer of electron density from an aromatic to the quinoid fragment of the EB tetramer. There is a second visible transition from one of the lower-energy occupied MOs to LUMO. It has the same nature: upon excitation, the electron density shifts from one of the adjacent cycles to the quinoid part of the tetramer. Molecular orbitals of aniline are not involved in any of the visible transitions.

The LWT in the EB−aniline clusters spans a broad region of almost 200 nm and the redshift is always concomitant with loss of intensity. It would be noteworthy to reveal which factors govern the visible absorption responsible for the polymer color. By comparing the results collected in Tables 1 and 2, one can conclude that UV/vis spectra are affected mostly by the in-core alignment of aniline, particularly in the vicinity of the quinoid ring and the imine nitrogen closer to the NH_2-capped end of the oligomer. The optimum separation of the two molecules for largest optical effect is about 4 Å, leading to total energy closer to the lowest and repulsion around the average values. Apparently, the mean twisting is not indicative because the average values of Θ differ substantially in the two aniline locations featuring the strongest redshift.

Analysis of the stacks frontier orbitals shows that in all cases the three highest occupied MOs are almost degenerate and are separated from the lower-energy occupied orbitals by a substantial energy gap (~1.1 eV). The LUMO orbital is also low-lying in the band gap, spaced from the rest of the virtual MOs (~1.5 eV, Figure 6).

The three highest-occupied MOs can interchange their position depending on the interaction with aniline, but HOMO is always one of the two orbitals originating from the EB tetramer. One of the latter is localized mainly on the second aniline moiety within the tetramer (A2) (HOMO−1 in Figure 6) and the other on the fourth aniline unit (A4) (HOMO in Figure 6). Therefore, the perturbation on the spectrum should be enhanced when aniline is located over A2, A3, and the quinoid ring because these are the fragments of the EB tetramer involved most efficiently in the LWT transition.

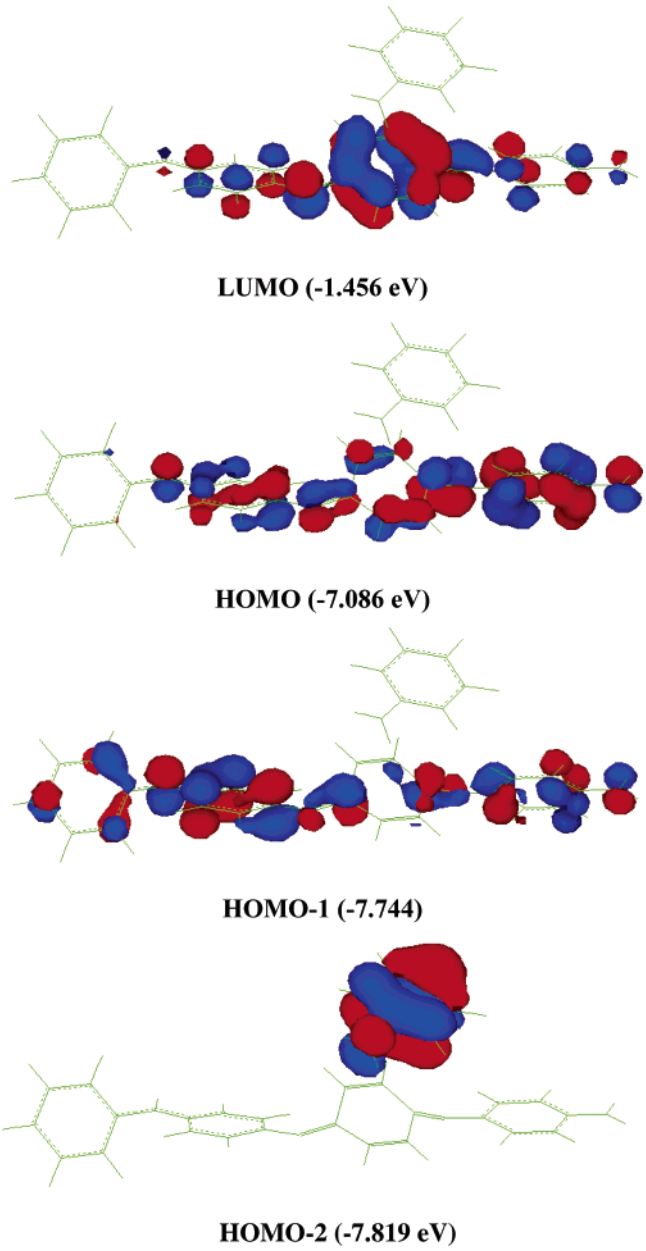

Figure 6. Frontier AM1 molecular orbitals of the EB−ANI−BQ optimized cluster. Red color corresponds to positive and blue color corresponds to negative sign. All plots are made at contour value 0.035. The water molecules are not shown. The energy of each orbital is given in brackets next to its notation.

Moreover, the wavelength of the LWT should depend on the possibility of effective electron transfer between A2 or A3 (depending on the nature of HOMO) and the quinoid cycle, that is, λ_{max} should be correlated with the torsion angle between the quinoid ring and A2 (A3). The values of these torsion angles are collected in Table 2.

Indeed, Θ_{QA} values are much larger for EB−ANI−BQ and EB−ANI−BN3, which feature the most pronounced redshift. This is an indication of enhanced interaction between the frontier orbitals of aniline and EB, which results in higher energy of HOMO (originating from EB) and lower energy of the aniline orbital, which becomes HOMO−2 in EB−ANI−BQ and EB−ANI−BN3. The occupied frontier orbital localized on aniline is HOMO−1 in all other clusters studied. This can be illustrated by the HOMO energies of the different clusters (Table 1). It is seen that EB−ANI−BQ and EB−ANI−BN3 have the highest E_{HOMO} value, combined with the most substantial torsion angles,

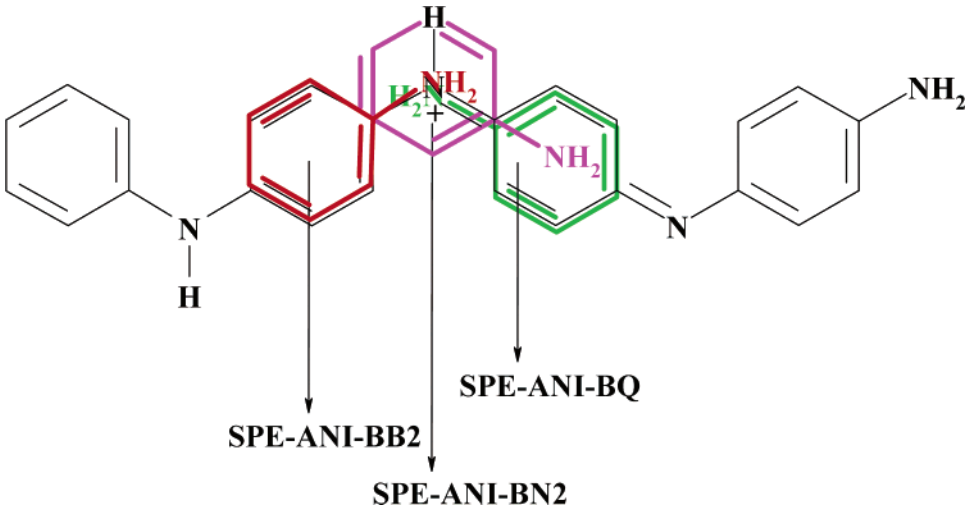

Figure 7. Scheme of the simulated SPE−ANI clusters. Different colors of the aniline molecule correspond to different alignment with respect to the tetramer.

Θ_{QA}, followed by EB−ANI−BN1, which are the three structures with lowest-energy LWT. It is noteworthy that, unlike HOMO, the energy of LUMO is not affected by the enhanced EB−aniline interaction.

Thus, the redshift of the LWT requires two conditions to be operative simultaneously: *strong* aniline-tetramer interaction and *proper spatial orientation* (nonbonding) of the frontier MOs of aniline and the tetramer.

2. Singly Protonated Emeraldine/Aniline Clusters. The same computational approach is applied to simulate structure and optical spectra of hydrated clusters of one singly protonated emeraldine (SPE) tetramer interacting with one aniline monomer. The optimized structures shown in Figure 8 are obtained for the three types of clusters.

The protonation site (Figure 1) is determined from the AM1 Mulliken atomic charges of a free EB tetramer.[32] Chloride anions are chosen as counterions because hydrochloric acid is often used as the protonating agent in experiments.[9,43]

The simulations with neutral clusters described in Section 1 lead to the conclusion that aniline perturbs oligomer properties substantially when it is in the locality of the quinoid cycle. In protonated species, aniline is expected to interact most intensely with the protonated imino nitrogen and its vicinity. Therefore, three types of SPE−aniline clusters are addressed (Figure 7).

The relevant structural characteristics are summarized in Table 3. Monte Carlo relaxation of the three starting structures followed by AMBER96 optimization of the selected series yield very dissimilar geometries. The most stable cluster is SPE−ANI−BN2, in which the aniline molecule is almost completely displaced from the tetramer, resulting in a strong interaction between the two nitrogens (from aniline and from SPE) and the hydrogens bound to them. To ease the repulsion of the latter, an appreciable tilt in the position of the aniline molecule versus the underlying ring is witnessed. This is due to enhanced heave of the proton (atomic charge +0.259) to the negative aniline nitrogen (atomic charge −0.412). Even though quite weak, in this case the binding between aniline and the SPE tetramer is already attractive, reflected in the negative value of the binding energy (the corresponding position in the neutral EB−ANI cluster features the highest positive binding energy of all of the neutral structures). This is in line with the shortest intermolecular distance between the two molecules and with the largest separation of the chloride anion from the cluster.

The other two structures, SPE−ANI−BB2 and SPE−ANI−BQ, have similar total energies, which are 25.7 and 34.2 kcal/mol higher, respectively. Moreover, the binding energies are repulsive in both cases. The binding energy in SPE−ANI−BB2 has not changed compared to the neutral cluster, but the energy in SPE−ANI−BQ is even more positive than that in the neutral structure. This gives definite preference to structures where aniline couples with the protonated nitrogen atom. The unfavorable interaction between aniline and SPE in the other two structures is compensated by a stronger attraction of the chloride anion from the proton, the distance being ∼3 Å. The location of the chloride anion with respect to the stack is also very different in SPE−ANI−BB2 and SPE−ANI−BQ than in SPE−ANI−BN2. Although in the latter Cl^- is away from the stack, in the other two structures it is located between the two nitrogen atoms (of aniline and of SPE) at almost equal distances, bridging them effectively to reduce the repulsion. In SPE−ANI−BB2, the aniline aromatic cycle remains on top of the SPE benzene ring but it is repelled at a distance of ∼6 Å. In SPE−ANI−BQ the two overlapping cycles are considerably displaced, which allows them to sustain relatively short intermolecular separation, that is, when no carbon atoms screen each other directly the interaction is less repulsive and hence the two rings can draw closer.

The average torsion angles are smaller than those in the corresponding EB−ANI clusters. However, the values in SPE−ANI−BN2 and SPE−ANI−BB2 are larger than both the average torsion angle of a single hydrated SPE tetramer (47.8°)[32] and Θ in a stack of two hydrated SPE tetramers (53.7°).[32] SPE−ANI−BQ, however, features a much more "flattened" structure, which should influence the electronic spectrum of this species.

The calculated visible transitions in the absorption spectra of the three types of SPE−aniline clusters are shown in Table 4 and Figure 5.

In all cases, the longest wavelength transition remains very intensive. The LWTs predicted for all types of SPE−ANI structures are strongly redshifted with respect to the single hydrated SPE tetramer and to the stack of two SPE tetramers in water.[32] However, the nature of the LWT is preserved; the electron transfer is localized within the SPE tetramer. Therefore, the presence of aniline only induces the redshift of this transition. The values are still lower than the experimental absorption of ∼820 nm, but this is due to the short oligomers studied. Another possible source of error may be inadequate account of the aqueous environment. However, this hypothesis was ruled out by test calculations on the same structures in vacuum. These

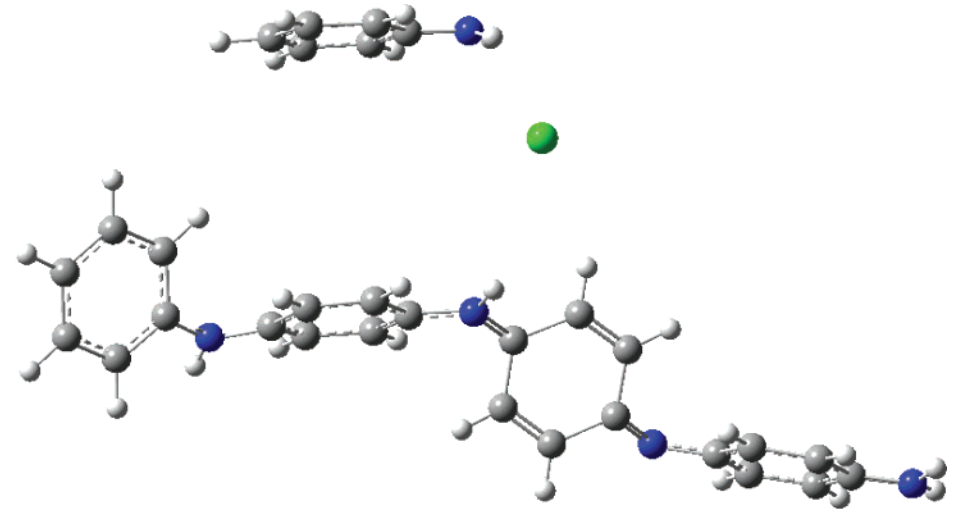

SPE-ANI-BB2

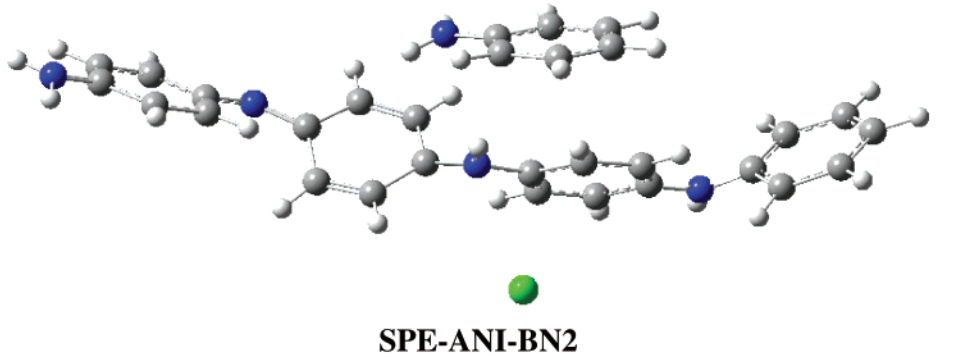

SPE-ANI-BN2

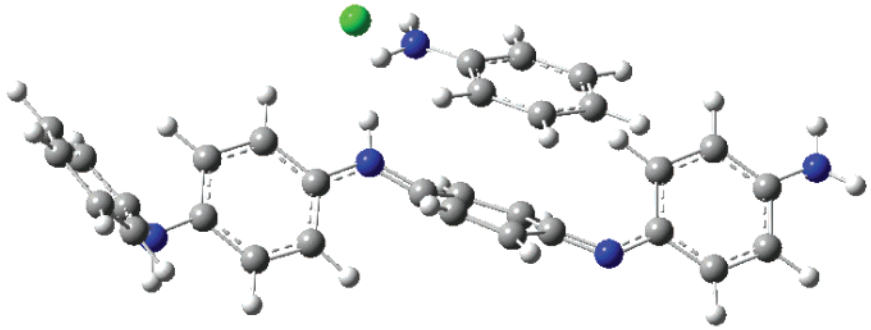

SPE-ANI-BQ

Figure 8. Illustrative examples of AMBER96 optimized structures of SPE−aniline stacks with different location of the aniline molecule on top of the SPE tetramer. The water molecules are not shown. The green sphere is the chloride anion.

produced different spectra (hypsochromically shifted) than those in the fixed field created by the water molecules and thus this is not the reason for lower computed wavelengths. In summary, the results are much closer to the experiment than the ones obtained just by accounting for the effect of water, protonation, and interaction with neighboring oligomers. The LWT is also bathochromically shifted relative to the corresponding neutral EB−ANI structures for SPE−ANI−BB2 and SPE−ANI−BN2 but hypsochromically in SPE−ANI−BQ. This is in line with the different interaction pattern of aniline with the singly protonated tetramer.

In SPE−ANI−BB2 and SPE−ANI−BN2, the LWT corresponds to transfer of electron density mainly from A2 to the quinoid ring and to the protonated nitrogen atom but in SPE−ANI−BN2 there are contributions from the other aromatic fragments: A1, A2, and A3. Nevertheless, λ_{max} is almost the same in the two clusters. This is a result of the interplay of the very similar values of the two competing factors: E_{HOMO} and twisting Θ_{QA} in the SPE−ANI−BB2 and SPE−ANI−BN2 tetramers (Table 4).

The blueshift in SPE−ANI−BQ can be explained by the fact that the structure is considerably flattened, which enhances delocalization and thus opens a broader band gap due to depression of bonding MOs at almost intact position of the frontier virtual ones (Table 4).

A special feature appears in the SPE−ANI−BQ simulated absorption spectrum, which is not observed in the other structures studied so far. A new visible transition arises at 611 nm, which is a charge transfer transition from aniline to the quinoid ring/protonated nitrogen moiety of the tetramer. It is

TABLE 4: AM1/CIS Calculated UV/Vis Spectra of SPE−Aniline Stacks in Water[a]

structure	λ, nm	f	MOs	E_i, eV	Θ_{QA}, deg
SPE−ANI−BB2	747 (39)	1.171 (0.146)	HOMO → LUMO	−7.477	67.00
	465 (16)	0.249 (0.119)	HOMO−5 → LUMO		
SPE−ANI−BN2	744 (15)	1.242 (0.037)	HOMO−3 → LUMO HOMO−5 → LUMO	−7.335	63.55
	490 (7)	0.013 (0.004)	HOMO−5 → LUMO		
SPE−ANI−BQ	681 (10)	1.264 (0.152)	HOMO−1 → LUMO	−7.670	58.70
	611 (30)	0.135 (0.144)	HOMO−2 → LUMO		
	405 (6)	0.013 (0.005)	HOMO−5 → LUMO		

[a]Only the wavelengths (λ) of the transitions in the visible region are presented. f is the oscillator strength. The values are averaged over a series of 15 optimized hydrated clusters for each structure. The standard deviations are given in brackets. The fourth column contains the configurations with the largest contributions involved in the transition. The last column comprises the AM1 energies of the relevant occupied MOs (E_i) involved in the LWT transition and the values of the torsion angle between the quinoid and the adjacent (A2 or A3) aromatic ring (Θ_{QA}) (see the text).

enabled by the relatively small intermolecular separation combined with still substantial screening of the two benzene rings, which allows bonding overlap between the frontier occupied orbitals of aniline and SPE.

Summary

Analysis of the results obtained for all of the systems studied (emeraldine base tetramer−aniline clusters and singly protonated emeraldine−aniline clusters) reveals that the excess of aniline monomers in the reaction medium during polymerization has a strong impact on the structure and the optical properties of PANI oligomers.

Examination of the energy of the studied systems shows that the interaction between aniline and emeraldine base is nonbonding, the repulsion being weaker at the quinoid/imino nitrogen fragment. On the contrary, coupling between aniline and the protonated nitrogen in SPE is already attractive. This implies that the presence of aniline in the reaction medium will facilitate protonation of PANI in the emeraldine oxidation state.

Structural changes are expressed mainly in ca. 10% enhanced overall twist for both EB and SPE oligomers because of stacking with the monomer. However, the most favorable packing has an opposite effect on the underlying fragment of the two species: it augments twisting for EB and eases it for SPE.

The interaction with aniline always leads to a strong bathochromic shift of the longest-wavelength visible transition, but it remains the most intensive one in the visible spectrum. Depending on the aniline/tetramer alignment, the LWT may appear between 600 and 775 nm. An explanation of this behavior is provided, based on the conjugation of the tetramer quinoid moiety with the neighboring rings, which alters the frontier orbitals sequence pattern.

Protonation of one of the tetramer imino nitrogens results in more redshifted LWT, which becomes even more intensive but remains localized within the SPE tetramer. In one of the structures studied, even an intermolecular CT transition at ∼600 nm from aniline to the tetramer emerges. The latter can be considered as a "fingerprint" for the presence of aniline in partially protonated PANI samples.

The substantial bathochromic shift of the visible transitions of EB and SPE due to their interaction with aniline is an indication that the experimentally recorded optical spectra of these forms may not correspond solely to the intrinsic absorption of oligoaniline but also include contribution from its complexes with the monomer. However, this hypothesis has to be substantiated by simulation of larger oligomers (octamers or hexadecamers), where the oligomer/monomer molecular weight ratio will be much larger and the perturbation of aniline may become too weak. Nevertheless, we believe that the results obtained in this study provide new and useful insights into the structure, organization, energetics, and optical properties of solvated PANI oligomers.

Acknowledgment. This work was supported by the COST P12 project "Structuring of Polymers" in the framework of a Short Term Scientific Mission COST-STSM-P12-01216 (A.I.).

Supporting Information Available: Computational details, optimized bond lengths and torsion angles, AMBER force field parameters, and potential energy curves from the Monte Carlo simulations. This material is available free of charge via the Internet at http://pubs.acs.org.

References and Notes

(1) Wang, Z.; Scherr, E.; MacDiarmid, A.; Epstein, A. *Phys. Rev. B* **1992**, *45*, 4190.
(2) Mizoguchi, K.; Nechtschein, M.; Travers, J. *Synth. Met.* **1991**, *41*, 113.
(3) Rouleau, J.; Goyette, J.; Bose, T.; Singh, R.; Tandon, *R. Phys. Rev. B* **1995**, *52*, 4801.
(4) Chen, S.; Hwang, G. *Macromolecules* **1996**, *29*, 3950.
(5) Pruneanu, S.; Veress, E.; Marian, I.; Oniciu, L. *J. Mater. Sci.* **1999**, *34*, 2733.
(6) Chakraborty, M.; Mukherjee, D. C.; Mandal, B. M. *Langmuir* **2000**, *16*, 2482.
(7) Neudeck, A.; Petr, A.; Dunsch, L. *J. Phys. Chem. B* **1999**, *103*, 912.
(8) Roth, K.; Krinichnyi, V. *Makromol. Chem.* **1993**, *72*, 143.
(9) (a) Kon′kin, A.; Shtyrlin, V.; Garipov, R.; Aganov, A.; Zakharov, A.; Krinichnyi, V.; Adams, P.; Monkman, A. *Phys. Rev. B* **2002**, *66*, 075203. (b) Krinichnyi, V.; Chemerisov, S.; Lebedev, Y. *Phys. Rev. B* **1997**, *55*, 16233.
(10) Petr, A.; Neudeck, A.; Dunsch, L. *Chem. Phys. Lett.* **2005**, *401*, 130.
(11) Long, Y.; Chen, Z. J.; Wang, N. L.; Ma, Y. J.; Zhang, Z.; Zhang, L. J.; Wan, M. X.; *Appl. Phys. Lett.* **2003**, *83*, 1863.
(12) (a) Blanchet, G.; Fincher, C.; Gao, F. *Appl. Phys. Lett.* **2003**, *82*, 1290, (b) Baibarac, M.; Baltog, I.; Lefrant, S.; Mevellec, J. Y.; Chauvet, O. *Chem. Mater.* **2003**, *15*, 4149.
(13) Gangopadhyay, R.; De, A. *Chem. Mater.* **2000**, *12*, 608.
(14) (a) Li, W.; Wang, H.-L. *J. Am. Chem. Soc.* **2004**, *126*, 2278. (b) Granholm, P.; Paloheimo, J.; Stubb, H. *Phys. Rev. B* **1997**, *55*, 13658.
(15) Lin, Y. H.; Cui, X. L. *Chem. Commun.* **2005**, *17*, 2226.
(16) Niessen, J.; Schroder, U.; Rosenbaum, M.; Scholz, F. *Electrochem. Commun.* **2004**, *6*, 571.
(17) Mattioli-Belmonte, M.; Giavaresi, G.; Biagini, G.; Virgili, L.; Giacomini, M.; Fini, M.; Giantomassi, F.; Natali, D.; Torricelli, P.; Giardino, R. *Int. J. Artif. Organs* **2003**, *26*, 1077.
(18) (a) Prigodin, V.; Samukhin, A.; Epstein, A. *Synth. Met.* **2004**, *141*, 155. (b) Joo, J.; Long, S.; Pouget, J.; Oh, E. J.; MacDiarmid, A.; Epstein, A. *Phys. Rev. B* **1998**, *57*, 9567. (c) Kohlman, R.; Zibold, A.; Tanner, D.; Ihas, G.; Ishiguro, T.; Min, Y.; MacDiarmid, A.; Epstein, A. *Phys. Rev. Lett.* **1997**, *78*, 3915. (d) Angelopoulos, M.; Ray, A.; MacDiarmid, A.; Epstein, A. *Synth. Met.* **1987**, *21*, 21.
(19) (a) Hong, S.; Park, S. *J. Phys. Chem. B* **2005**, *109*, 9305. (b) Luthra, V.; Singh, R.; Gupta, S.; Mansingh, A. *Curr. Appl. Phys.* **2003**, *3*, 219.
(20) McManus, P.; Cushman, R.; Yang, S. *J. Phys. Chem.* **1987**, *91*, 744.

(21) Stafstroem, S.; Bre'das, J. L.; Epstein, A. J.; Woo, H. S.; Tanner, D.; Huang, W. S.; MacDiarmid, A. *Phys. Rev. Lett.* **1987**, *59*, 1464.

(22) (a) Aksimentyeva, O.; Konopelnik, O. *Mol. Cryst. Liq. Cryst.* **2005**, *427*, 429. (b) Sarno, D.; Manohar, S.; MacDiarmid, A. *Synth. Met.* **2005**, *148*, 237. (c) Wu, C. G.; Chang, S. S. *J. Phys. Chem. B* **2005**, *109*, 825.

(23) Kulkarni, M.; Viswanath, A.; Marimuthu, R.; Seth, T. *Polym. Eng. Sci.* **2004**, *44*, 1676.

(24) Sahoo, S.; Nagarajan, R.; Roy, S.; Samuelson, L. A.; Kumar, J.; Cholli, A. L. *Macromolecules* **2004**, *37*, 4130.

(25) (a) Jayakannan, M.; Annu, S.; Ramalekshmi, S. *J. Polym. Sci., Part B: Polym. Phys.* **2005**, *43*, 1321. (b) Krinichnyi, V.; Tokarev, S. *Polymer Science Series A* **2005**, *47*, 261. (c) Pouget, J.; Jozefowicz, M.; Epstein, A.; Tang, X.; MacDiarmid, A. *Macromolecules* **1991**, *24*, 779.

(26) de Oliveira, Z. T., Jr.; dos Santos, M. *Chem. Phys.* **2000**, *260*, 95.

(27) Foreman, J. P.; Monkman, A. P. *J. Phys. Chem. A* **2003**, *107*, 7604.

(28) Libert, J.; Cornil, J.; dos Santos, D. A.; Bredas, J. L. *Phys. Rev. B* **1997**, *56*, 8638.

(29) Ikkala, O.; Mietila, L.-O.; Ahjopalo, L.; Oesterholm, H.; Passiniemi, P. J. *J. Chem. Phys.* **1995**, *103*, 9855.

(30) Vaschetto, M.; Ratamal, B. *J. Phys. Chem. A* **1997**, *101*, 6945.

(31) Cornil, J.; dos Santos, D. A.; Crispin, X.; Silbey, R.; Bredas, J. L. *J. Am. Chem. Soc.* **1998**, *120*, 1289.

(32) Ivanova, A.; Madjarova, G.; Tadjer, A.; Gospodinova, N. *Int. J. Quantum Chem.*, in press (available online), 2006.

(33) Gospodinova, N.; Mokreva, P.; Terlemezyan, L. *Polym. Int.* **1996**, *41*, 79.

(34) Cushman, R. J.; McManus, P. M.; Yang, S. Ch. *J. Electroanal. Chem.* **1986**, *291*, 335.

(35) Agbor, N. E.; Petty, M. C.; Monkman, A. P.; Harris, M. *Synth. Met.* **1993**, *55*−*57*, 3789.

(36) Goldenberg, L. M.; Petty, M. C.; Monkman, A. P. *Electrochem. Soc.* **1994**, *141*, 1573.

(37) *HyperChem 7.0 Reference Manual*; Hypercube Inc.: Gainsville, FL, 2002.

(38) *HyperChem 7.0*; Hypercube Inc.: Gainsville, FL.

(39) Metropolis, N.; Rosenbluth, A. W.; Rosenbluth, M. N.; Teller, A. H.; Teller, E. *J. Chem. Phys.* **1953**, *21*, 1087.

(40) (a) Weiner, S. J.; Kollman, P. A.; Case, D. A.; Singh, U. C.; Ghio, C.; Alagona, G.; Profeta, S., Jr.; Weiner, P. *J. Am. Chem. Soc.* **1984**, *106*, 765. (b) Weiner, S. J.; Kollman, P. A.; Nguyen, D. T.; Case, D. A. *J. Comput. Chem.* **1986**, *7*, 230. (c) Cornell, W. D.; Cieplak, P.; Bayly, C. I.; Gould, I. R.; Merz, K. M., Jr.; Ferguson, D. M.; Spellmeyer, D. C.; Fox, T.; Caldwell, J. W.; Kollman, P. A. *J. Am. Chem. Soc.* **1995**, *117*, 5179.

(41) Jorgensen, W. L.; Chandrasekhar, J.; Madura, J. D.; Impey, R. W.; Klein, M. L. *J. Chem. Phys.* **1983**, *79*, 926.

(42) (a) Enkelmann, V.; Morra, B.; Krohnke, C.; Wegner, G.; Heinze, J. *Chem. Phys.* **1982**, *66*, 303. (b) Enkelmann, V. *Adv. Chem.* **1988**, *217*, 177.

(43) Jing, L.; Fang, K.; Hong, Q.; Li, S.; Mao, W. *Synth. Met.* **2004**, *142*, 107.